PHYSICAL REVIEW B **90**, 054421 (2014)

# Improvement of magnetic hardness at finite temperatures: *Ab initio* disordered local-moment approach for YCo$_5$

Munehisa Matsumoto,[1] Rudra Banerjee,[2] and Julie B. Staunton[2]

[1]*Elements Strategy Initiative Center for Magnetic Materials (ESICMM), National Institute for Materials Science, Tsukuba 305-0047, Japan*

[2]*Department of Physics, University of Warwick, Coventry CV4 7AL, United Kingdom*

(Received 22 May 2014; revised manuscript received 4 August 2014; published 26 August 2014)

Temperature dependence of the magnetocrystalline anisotropy energy and magnetization of the prototypical rare-earth magnet YCo$_5$ is calculated from first principles, utilizing the relativistic disordered local-moment approach. We discuss a strategy to enhance the finite-temperature anisotropy field by hole doping, paving the way for an improvement of the coercivity near room temperature or higher.

DOI: 10.1103/PhysRevB.90.054421 PACS number(s): 75.30.Gw, 75.50.Ww, 75.10.Lp, 71.15.Rf

## I. INTRODUCTION

Ferromagnetism in permanent magnets has been a long-standing problem in solid-state physics and materials science. The mechanism of coercivity, resistance of the spontaneous magnetization against the externally applied magnetic field in the reverse direction, is not yet entirely known after almost 70 years since Brown's paradox [1]. Development of modern rare-earth magnets such as Nd$_2$Fe$_{14}$B [2] and SmCo$_5$ [3,4] triggered material-specific investigations of the coercivity mechanism [5]. They culminate in today's state-of-the-art technological optimization of the microstructure of ferromagnetic materials for the enhanced coercivity [6] on the phenomenological and empirical basis. More fundamental understanding and controlling on the basis of solid-state physics and statistical physics is desired to better use these technological advances. Especially the temperature decay of coercivity is a problem in industrial applications and thus more and more demands for the control of finite-temperature properties of permanent magnets are rising.

The high-temperature tail of the magnetism is mostly carried by 3$d$ electrons [7] in the intermetallic system between transition-metal and rare-earth (RE) elements while the low-temperature magnetism is dominated by 4$f$ electrons. Thus developing an understanding and the theoretical control over the temperature decay of 3$d$-electron magnetism has the universal utility for the optimization of high-temperature magnetism of RE magnets. Thus we focus on YCo$_5$ as our target system, extracting the 3$d$-electron part out of the SmCo$_5$ family. The so-called 1-5 magnets represent the RE magnets with one of the simplest crystal structures and SmCo$_5$-based magnets are second in magnetic performance only to the champion-magnet family including Nd$_2$Fe$_{14}$B; SmCo$_5$ currently serves for some special applications under extreme conditions [8] with its high Curie temperature and stability against corrosion. Also the large magnetocrystalline anisotropy energy (MAE) of 5.5 MJ/m$^3$ at room temperature $T = 295$ K in YCo$_5$ [9] can let itself qualify for permanent magnet applications [8].

Describing the magnetic properties of such a material presents significant challenges to *ab initio* theory. Itinerant electron magnetism in realistic magnetic materials has often been addressed in the ground state with the application of the density-functional theory (DFT). Incorporation of finite temperature physics and description of correlated electron behavior can be issues for DFT which does not always include localized electron effects adequately into its scope. Both issues require a combination of DFT and statistical physics in some way. Here we follow the idea of disordered local moments [10–13] to incorporate the physics of thermal fluctuations of well-developed magnetic moments into the spin-polarized DFT for ferromagnetic materials [14–17]. A relativistic version of the disordered local-moment (DLM) approach has recently been developed [18,19] and successfully applied to finite-temperature magnetic anisotropy in L1$_0$-FePt alloys [18,19] and Co films [20] where magnetism is all carried by $d$ electrons. Thus the $d$-electron part in the magnetism of rare-earth magnets can be a good target for DLM.

In this work we present *ab initio* calculations based on DLM for YCo$_5$ at finite temperatures. From calculated temperature dependence of the magnetization $M$ and the MAE, which we denote by $K_{\mathrm{u1}}$ as it mostly comes from the uniaxial magnetocrystalline anisotropy (MCA) for YCo$_5$, we address the thermal decay of the anisotropy field estimated as $H_{\mathrm{A}} = 2K_{\mathrm{u1}}/M$ which generally shows the approximate proportionality to the coercivity field $H_{\mathrm{c}}$ [21]. The relation is practically $H_{\mathrm{c}} \sim 0.2H_{\mathrm{A}}$ with the practical hard upper limit being $H_{\mathrm{c}} \lesssim 0.5H_{\mathrm{A}}$ that is reached only in some exceptional samples [22]. Assuming such rough proportionality, we propose a strategy to improve $H_{\mathrm{A}}(T)$ at high temperatures in the range $T \sim 400$–$500$ K. Our main message is encapsulated in Fig. 1 which shows that hole-doped YCo$_5$ with the number of doped holes being 0.24 and 0.35 per unit cell has the stronger anisotropy field than pure YCo$_5$ in the temperature range $T \gtrsim 450$ K and $T \gtrsim 550$ K, respectively.

Experimentally, doping-enhanced coercivity has been known for YCo$_{5-x}$Ni$_x$ and other RECo$_{5-x}$Cu$_x$ magnets (RE = Ce, Sm) [28]. The coercivity is indeed significantly affected by doping, which is seen in our calculated results on the filling dependence of MAE near the ground state as shown in Fig. 2. On top of such a filling dependence of coercivity determined by the electronic structure, our idea is to let the electronic states below the peak of MAE in Fig. 2 be thermally populated so that the high-temperature MAE is enhanced. Experimentally observed doping-enhanced coercivity had been discussed in conjunction with intrinsic pinning [28]. Our results on the finite-temperature physics together with the electron-band-filling-sensitive nature of MAE point to a new scenario for doping-enhanced coercivity at high temperatures.

©2014 American Physical Society

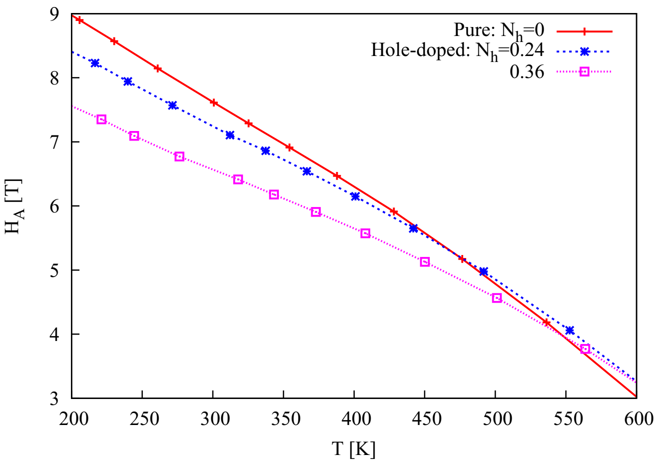

FIG. 1. (Color online) Calculated temperature dependence of the anisotropy field $H_\mathrm{A}$ for pure and hole-doped $\mathrm{YCo}_5$, where doping-induced enhancement of $H_\mathrm{A}$ is observed in the temperature range $T \gtrsim 450$–$550$ K with the number of doped holes being $N_h = 0.24$ and 0.36, respectively.

The rest of the paper is organized as follows. Our proposal on the strategy to enhance the high-temperature coercivity is found in Sec. IV. This follows an outline of the DLM methodology underpinning the calculations in Secs. II and III. Conclusions are given in Sec. V.

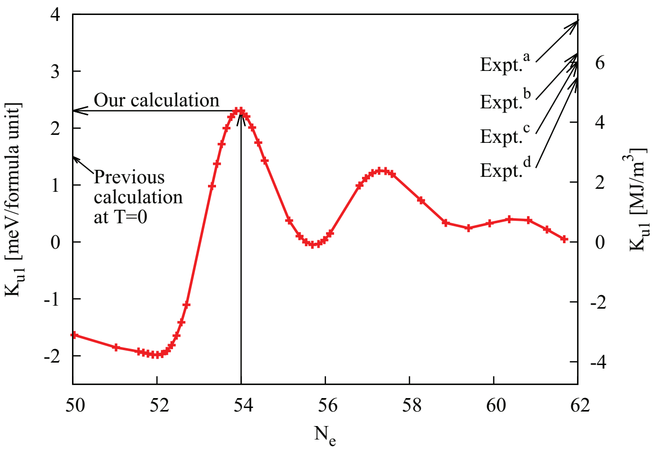

FIG. 2. (Color online) Calculated magnetic anisotropy energy plotted as the function of the valence electron number for $\mathrm{YCo}_5$ near the ground state $T = 0$ K. The numbers on the left-hand side of the vertical axis indicate the results per the formula unit of $\mathrm{YCo}_5$ and those on the right-hand side of the vertical axis give the same quantities converted to per the unit volume using the experimental lattice constants in Ref. [26]. The previous theoretical result for MAE at $T = 0$ is taken from Ref. [27]. The number of valence electrons per formula unit of $\mathrm{YCo}_5$ is 54 (a, $K_{\mathrm{u}1} = 7.38$ MJ/m$^3$ at $T = 4.2$ K from Ref. [23]; b, $K_{\mathrm{u}1} = 6.3$ MJ/m$^3$ at $T = 77$ K from Ref. [24]; c, $K = 6.03$ MJ/m$^3$ from Ref. [25] at $T = 293$ K. We assume $K_{\mathrm{u}1}$ dominates in $K$ as was shown in Ref. [23], and d, $K_{\mathrm{u}1} = 5.5$ MJ/m$^3$ at room temperature from Ref. [8]).

## II. METHODS

Our computational method, the DLM approach, is based on the Korringa-Kohn-Rostoker (KKR) method [29,30] and coherent potential approximation (CPA) [31] for *ab initio* electronic structure calculations. Especially to address the temperature dependence of MAE which is brought about by spin-orbit interaction (SOI), we follow the relativistic formulation [18,19]. These aspects in Secs. II A and II B, describe the general framework and how to extract MAE, respectively, at the level of sketching the basic ideas. The MAE as our key observable is focused on and for the rest of the observables that we present in Sec. III, we refer to the original works [15,19] and a recent review article [32] for their explicit expressions in terms of KKR-CPA. In Sec. II C we give the details of the application to the case of $\mathrm{YCo}_5$.

### A. Framework

#### 1. *Separation of fast and slow dynamics*

Under the situation that spin-fluctuation dynamics are much slower than the characteristic time scales of electronic motions [15], well-developed classical local moments $\hat{\mathbf{e}}$ are assumed to exist on each site $i = 1 \cdots N$ in the unit cell, with $N$ being the number of magnetic atoms in the unit cell. The thermal average $\langle\,\rangle$ of the local moment

$$\langle \hat{\mathbf{e}}_i \rangle = \int \cdots \int \hat{\mathbf{e}}_i\, P^{(\hat{n})}(\{\hat{\mathbf{e}}\}) d\,\hat{\mathbf{e}}_1 \cdots d\,\hat{\mathbf{e}}_N \tag{1}$$

is assumed to be aligned with the magnetization direction $\hat{\mathbf{n}}$ for a ferromagnet. Here $\hat{\mathbf{n}}$ is fixed in the calculation by hand. We have specified the configuration of the local moments by $\{\hat{\mathbf{e}}\}$ and statistical weight $P^{(\hat{n})}(\{\hat{\mathbf{e}}\})$ given in terms of the Boltzmann weights at finite temperatures. $\langle \hat{\mathbf{e}}_i \rangle = \mathbf{m}_i$ is a magnetic order parameter. For a ferromagnet, magnetized along a direction $\hat{\mathbf{n}}$, $\mathbf{m}_i = m_i \hat{\mathbf{n}}$.

#### 2. *DLM as a realistic mean-field theory*

DLM is implemented as a realistic mean-field theory for the local moments embedded in a sea of electrons given by spin-polarized DFT for the target material. For a given configuration of the local moments

$$\{\hat{\mathbf{e}}\} \equiv \{\hat{\mathbf{e}}_1, \hat{\mathbf{e}}_2, \ldots, \hat{\mathbf{e}}_N\},$$

the Boltzmann weight is defined as

$$\exp\big[-\beta\Omega^{(\hat{\mathbf{n}})}(\{\hat{\mathbf{e}}\})\big],$$

referring to the grand potential $\Omega^{(\hat{\mathbf{n}})}(\{\hat{\mathbf{e}}\})$ in the spin-resolved density functional theory for a given target ferromagnet ($\beta = 1/k_B T$). The partition function is accordingly written as

$$Z^{(\hat{\mathbf{n}})} = \int \cdots \int \exp\big[-\beta\Omega^{(\hat{\mathbf{n}})}(\{\hat{\mathbf{e}}\})\big] d\,\hat{\mathbf{e}}_1 \cdots d\,\hat{\mathbf{e}}_N$$

and the probability distribution function (PDF) in Eq. (1) of the local-moment configuration $\{\hat{\mathbf{e}}\}$ is

$$P^{(\hat{\mathbf{n}})} = \frac{\exp\big[-\beta\Omega^{(\hat{\mathbf{n}})}(\{\hat{\mathbf{e}}\})\big]}{Z^{(\hat{\mathbf{n}})}}.$$

Here we use the mean-field approximation (MFA)

$$\Omega_0^{(\hat{\mathbf{n}})}(\{\hat{\mathbf{e}}\}) \overset{\text{MFA}}{=} \sum_{i=1}^{N} \mathbf{h}_i^{(\hat{\mathbf{n}})} \cdot \hat{\mathbf{e}}_i, \tag{2}$$

where the Weiss field $\mathbf{h}_i^{(\hat{\mathbf{n}})} = h_i^{(\hat{\mathbf{n}})}\hat{\mathbf{n}}$ is written as follows [15]:

$$h_i^{(\hat{\mathbf{n}})} = \int \frac{3}{4\pi}(\hat{\mathbf{e}}_i \cdot \hat{\mathbf{n}})\langle \Omega^{(\hat{\mathbf{n}})}\rangle_{\hat{\mathbf{e}}_i} d\,\hat{\mathbf{e}}_i \tag{3}$$

for $i = 1 \cdots N$ where $i$ runs over the local moments in the unit cell and the thermal average denoted by $\langle\cdot\rangle_{\hat{\mathbf{e}}_i}$ implies the restriction in the averaging process with the direction of the local moment on site $i$ fixed to that specified by $\hat{\mathbf{e}}_i$. [Further terms proportional to, say, $(\hat{\mathbf{e}}_i \cdot \hat{\mathbf{n}})^2$, can be added to Eq. (2) to improve the mean-field description [41] but have a rather small effect.] With the MFA in Eq. (2) the overall partition function factorizes into contributions from each of local moments

$$Z^{(\hat{\mathbf{n}})} = \prod_{i=1}^{N} Z_i^{(\hat{\mathbf{n}})}$$

and the partition function is written in terms of the Weiss field

$$\begin{aligned} Z_i^{(\hat{\mathbf{n}})} &= \int \exp\left(-\beta \mathbf{h}_i^{(\hat{\mathbf{n}})} \cdot \hat{\mathbf{e}}_i\right) d\,\hat{\mathbf{e}}_i \\ &= \frac{4\pi}{\beta h_i^{(\hat{\mathbf{n}})}} \sinh \beta h_i^{(\hat{\mathbf{n}})} \end{aligned} \tag{4}$$

and the PDF is written as follows:

$$\begin{aligned} P_i^{(\hat{\mathbf{n}})}(\hat{\mathbf{e}}_i) &= \exp\left(-\beta \mathbf{h}_i^{(\hat{\mathbf{n}})} \cdot \hat{\mathbf{e}}_i\right)/Z_i^{(\hat{\mathbf{n}})} \\ &= \frac{\beta h_i^{(\hat{\mathbf{n}})}}{4\pi \, \sinh \beta h_i^{(\hat{\mathbf{n}})}} \exp\left(-\beta \mathbf{h}_i^{(\hat{\mathbf{n}})} \cdot \hat{\mathbf{e}}_i\right). \end{aligned} \tag{5}$$

With this expression for the PDF, the free energy is written as follows:

$$F^{(\hat{\mathbf{n}})} = \langle \Omega^{(\hat{\mathbf{n}})}\rangle + \frac{1}{\beta}\sum_{i=1}^{N}\int P_i^{(\hat{\mathbf{n}})}(\hat{\mathbf{e}}_i)\log\, P_i^{(\hat{\mathbf{n}})}(\hat{\mathbf{e}}_i) d\,\hat{\mathbf{e}}_i, \tag{6}$$

where the first term describes the internal energy and the second describes $-TS$ with the magnetic entropy

$$S = -k_B \sum_{i=1}^{N}\int P_i^{(\hat{\mathbf{n}})}(\hat{\mathbf{e}}_i)\log\, P_i^{(\hat{\mathbf{n}})}(\hat{\mathbf{e}}_i) d\,\hat{\mathbf{e}}_i.$$

The magnetization is given using the PDF in Eq. (5) as follows:

$$\mathbf{m}_i^{(\hat{\mathbf{n}})} = \langle \hat{\mathbf{e}}_i \rangle \equiv m_i^{(\hat{\mathbf{n}})} \mathbf{h}_i^{(\hat{\mathbf{n}})}, \tag{7}$$

$$m_i^{(\hat{\mathbf{n}})} = -\frac{1}{\beta h_i^{(\hat{\mathbf{n}})}} + \coth \beta h_i^{(\hat{\mathbf{n}})} = L\left(\beta h_i^{(\hat{\mathbf{n}})}\right). \tag{8}$$

Here $L(x)$ is the Langevin function.

#### 3. *CPA to embed the thermal disorder into DFT*

CPA [31] is an approach to deal with the disorder physics on a mean-field level by averaging over the random potentials to introduce an effective uniformly distributed potential. Following the original idea by Hasegawa [11] and Hubbard [12], thermal disorder in local moments is embedded into the description of the electronic states [15] on the level of CPA.

The way that the CPA determines the effective medium is by letting the motion of an electron simulate the motion of an electron on the average. The scattering problem at the heart of KKR is solved to get the single-site $t$ matrix $\underline{t}_i$ for each local moment $i$ where the underlined $t$ matrix is that in orbital and spin angular momentum space. Some more elaboration on that solution is given below with Eq. (12). For the system magnetized along the direction $\hat{\mathbf{n}}$, the medium is specified by a set of CPA-imposed $t$ matrices [33]

$$\underline{\underline{t}}_c^{(\hat{\mathbf{n}})} \equiv (\underline{t}_{1,c}, \underline{t}_{2,c}, \ldots, \underline{t}_{N,c})$$

which is determined (for details we refer to Ref. [19]) for a given set of Weiss fields $h_i^{(\hat{\mathbf{n}})}$ as in Eq. (3) and corresponding $P_i^{(\hat{\mathbf{n}})}(\hat{\mathbf{e}}_i)$ as in Eq. (5), where the finite-temperature physics is encapsulated.

The $t$ matrices $\underline{\underline{t}}_c^{(\hat{\mathbf{n}})}$ that specify the effective medium comes into the formulation of DFT as follows. By magnetic force theorem we consider only the single-particle energy part of the spin-resolved DFT grand potential as our effective local-moment Hamiltonian

$$\Omega^{(\hat{\mathbf{n}})}(\{\hat{\mathbf{e}}\}) \simeq -\int dE\, f_{\text{FD}}(E;\mu^{(\hat{\mathbf{n}})}) N^{(\hat{\mathbf{n}})}(E;\{\hat{\mathbf{e}}\}), \tag{9}$$

where $f_{\text{FD}}(E;\mu^{(\hat{\mathbf{n}})})$ is the Fermi-Dirac distribution function with the chemical potential being $\mu^{(\hat{\mathbf{n}})}$ and $N^{(\hat{\mathbf{n}})}(E;\{\hat{\mathbf{e}}\})$ is the integrated density of states [19,34] with the given direction of magnetization $\hat{\mathbf{n}}$ and the given configuration of local moments $\{\hat{\mathbf{e}}\}$. Using the Lloyd formula [35] for $N^{(\hat{\mathbf{n}})}(E;\{\hat{\mathbf{e}}\})$ on the right-hand side of Eq. (9), the grand potential is expressed in terms of the $t$ matrices [19].

### B. Calculation of magnetic anisotropy energy

#### 1. *Defining the MAE for the uniaxial MCA*

For uniaxial magnets, the free energy takes the form

$$F^{(\hat{\mathbf{n}})} = F_{\text{iso}} + K_{\text{u1}} \sin^2\theta,$$

where $F_{\text{iso}}$ is the isotropic part, $K_{\text{u1}} > 0$ is the MAE for uniaxial MCA, and $\theta$ is the angle between the direction of magnetization and the easy axis. Then

$$\begin{aligned} T_\theta &= -\frac{\partial F}{\partial \theta} \\ &= -2K_{\text{u1}}\sin\theta\,\cos\theta. \end{aligned} \tag{10}$$

Thus in order to extract MAE for the uniaxial MCA we fix the direction of magnetization to be $\hat{\mathbf{n}} = (1,0,1)/\sqrt{2}$, that is, $\hat{\mathbf{n}} = (\sin\theta\,\cos\phi, \sin\theta\,\sin\phi, \cos\theta)$ with $\theta = \pi/4$ and $\phi = 0$ and calculate the magnetic torque $T_{\theta=\pi/4}$. Our target MAE is obtained as

$$K_{\text{u1}} = -T_{\theta=\pi/4}. \tag{11}$$

#### 2. *Spin-orbit interaction in relativistic KKR*

For a given set of self-consistent potentials, electronic charge, and local-moment magnitudes, the directions of local moments are described by the unitary transformation of the single-site $t$ matrix for local moment $i$,

$$\underline{t}_i(E;\hat{\mathbf{e}}_i) = \underline{R}(\hat{\mathbf{e}}_i)\underline{t}_i(E;\hat{\mathbf{z}})\underline{R}(\hat{\mathbf{e}}_i)^\dagger, \tag{12}$$

where $\underline{t}(E;\hat{\mathbf{z}})$ is the $t$ matrix with the effective field pointing along the local $z$ axis for given energy $E$, and $\underline{R}(\hat{\mathbf{e}}_i)$ is for the $O(3)$ unitary transformation that rotates the $z$ axis along the direction of $\hat{\mathbf{e}}_i$. The scattering problem at the heart of KKR is solved incorporating spin-orbit interaction (SOI) with a magnetic field pointing along the $z$ axis [36] and the single-site $t$ matrix $\underline{t}_i(E;\hat{\mathbf{z}})$ is obtained.

In the absence of SOI, an element of the single-site scattering $t$ matrix

$$t_{i;l,m,\sigma;l',m',\sigma'} = t_{i;l,\sigma}\delta_{l,l'}\delta_{m,m'}. \tag{13}$$

where $l$ is the angular momentum quantum number and $m$ the azimuthal component, and

$$\underline{t}_i(E;\hat{\mathbf{e}}_i) = \underline{t}_i^+\underline{1} + \underline{t}_i^-\sigma\cdot\mathbf{e}_i, \tag{14}$$

where an element $t^{+(-)}_{l,m;l',m'} = \frac{1}{2}[t_{i;l,\frac{1}{2}} + (-)t_{i;l,-1/2}]$. When SOI is included, the $t$ matrix is no longer independent of $m$ which leads to the generation of magnetic anisotropic effects.

### 3. *Torque-based formula in KKR-CPA*

The uniaxial MAE is obtained as the derivative of the free energy following Eq. (10). Inserting Eq. (6) for the free energy, we get the following [19]:

$$T_\theta^{(\hat{\mathbf{n}})} = -\frac{\partial}{\partial\theta}\sum_i\int P_i^{(\hat{\mathbf{n}})}(\hat{\mathbf{e}}_i)\langle\Omega^{(\hat{\mathbf{n}})}\rangle_{\hat{\mathbf{e}}_i} d\,\hat{\mathbf{e}}_i. \tag{15}$$

This is our working formula to produce the results for the finite-temperature MAE of $\mathrm{YCo_5}$ which we now go on to describe.

## C. Specifics with the case of $\mathrm{YCo_5}$

The past decade has seen the successful application of DLM theory to $\mathrm{L1_0}$-FePt alloy [18,19] which is a uniaxial ferromagnet and the magnetism is carried largely by $3d$ and $5d$ electrons. Since $\mathrm{YCo_5}$ involves mostly $3d$ electrons for its magnetism, success of DLM description on the same level as was achieved for $\mathrm{L1_0}$-FePt is expected provided that the assumption of localized moment on the magnetic atoms works well. Some care must be taken in the application of DLM for Co-based magnets since the trend among Fe, Co, and Ni [13] shows that the assumption of localized moment works well for Fe, faces challenge for Ni, and Co sits somewhere in-between. Stability of local moments on the Co sublattices in the present case is discussed in Sec. II C 2. Indeed we will see below some inherent underestimate near the Curie point in our calculations which might indicate some fragile nature of the local moments in $\mathrm{YCo_5}$. This problem can be cured by extending the calculation to that based on the nonlocal CPA [37,38]. For now we are mostly concerned with the lowest-temperature properties and the middle-temperature range of $T \lesssim 600$ K which is well below the Curie temperature at $T_{\mathrm{Curie}} = 920$ K [26]. So we proceed with the single-site theory within the scope of the present project.

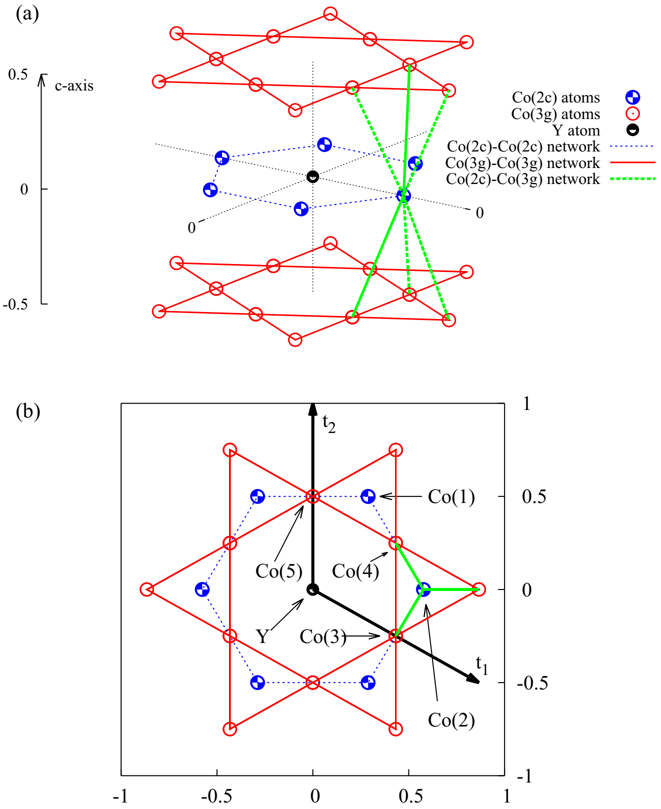

FIG. 3. (Color online) Crystal structure of $\mathrm{YCo_5}$: (a) bird's-eye view and (b) top view seen along the $c$ axis. Nearest-neighbor pairs in the Co($2c$)-Co($3g$) network are only partially drawn for the illustration. Labels for atoms in (b) follow Table I.

### 1. *Crystal structure*

We take the experimental crystal structure of $\mathrm{YCo_5}$ with the space group No. 191 $a = 4.948$ Å and $c = 3.975$ Å [26]. The unit cell consists of one formula unit: Y, Co($2c$), and Co($3g$) sublattices. The atomic configuration in the unit cell is shown in Fig. 3(a) as a bird's-eye view. The top view along the $c$ axis is shown in Fig. 3(b) to illustrate the relative positions of the Co($2c$) atoms and the Co($3g$) atoms. Within the layer along the $ab$ plane, it is seen that nearest-neighbor Co($3g$) atoms form a kagome lattice. Between those kagome layers, Co($2c$) atoms sit right on the center of Co($3g$) triangles to form a hexagonal lattice on the same $ab$-plane layer as Y atoms. The ratio $c/a \simeq 0.80$ means that the tetrahedron formed by the Co($3g$) triangle and the Co($2c$) atom is close to the regular one. So the Co($2c$)-Co($3g$) atomic distance is almost equal to the Co($3g$)-Co($3g$) distance which is $0.5a$. On the other hand, the Co($2c$)-Co($2c$) distance which is $a/\sqrt{3} \simeq 0.58a$ spans the longest distance among the nearest-neighbor Co atom pairs. We set the position of each atom and the direction of the translation vectors as shown in Table I in our calculation. The labeling scheme for the atoms and the directions is illustrated in Fig. 3(b).

### 2. *Robustness of local moments in $\mathrm{YCo_5}$*

We inspect the validity of the DLM approach at finite temperatures in the present calculation. Calculated temperature

TABLE I. Setup of the unit cell of $YCo_5$ in the present calculations.

| Sublattice | Atom | Atomic coordinates |
|---|---|---|
| Y | | (0,0,0) |
| Co(2c) | Co(1) | $(1/(2\sqrt{3}),1/2,0)$ |
| | Co(2) | $(1/\sqrt{3},0,0)$ |
| Co(3g) | Co(3) | $(\sqrt{3}/4,-1/4,1/2)$ |
| | Co(4) | $(\sqrt{3}/4,1/4,1/2)$ |
| | Co(5) | $(0,1/2,1/2)$ |
| Primitive translation vectors | | |
| $\mathbf{t}_1$ | $(\sqrt{3}/2,-1/2,0)$ | |
| $\mathbf{t}_2$ | $(0,1,0)$ | |
| $\mathbf{t}_3$ | $(0,0,1)$ | |

dependence of each of the local moments in $YCo_5$ are shown in Fig. 4. The DLM picture of magnetism in metals at finite temperature is based on the assumption that there are some aspects of the interacting electrons of a material that vary slowly in comparison with faster degrees of freedom. These are captured in terms of the orientational unit vectors, $\{\hat{\mathbf{e}}\}$, the transverse part of the magnetic fluctuations. The electronic grand potential $\Omega^{(\hat{\mathbf{n}})}(\{\hat{\mathbf{e}}\})$ is, in principle, available from spin-resolved DFT (SDFT) generalized for the noncollinear magnetic profiles which are labeled by $\{\hat{\mathbf{e}}\}$ [15]. Within the tenets of SDFT the charge and magnetization densities depend on these configurations, i.e., $\rho(\mathbf{r},\{\hat{\mathbf{e}}\})$, $\vec{M}(\mathbf{r},\{\hat{\mathbf{e}}\})$. In the space around an atom at a site $i$ the magnetization is constrained to follow the orientation $\hat{\mathbf{e}}_i$ there but its magnitude $\mu(\mathbf{r})$ can depend on the surrounding orientational environment, $\mu(\mathbf{r}) = \mu(\mathbf{r},\{\hat{\mathbf{e}}\})$. In many of the materials where the DLM theory has been successfully applied, the magnitudes are found to be rather insensitive to the environment and can be modeled accurately as rigid local moments. In other materials, e.g., Ni [39], the magnetism is driven by the coupling of the magnitudes (longitudinal magnetic fluctuations) with these transverse modes. When there is short-range aligning of the orientations or long-range magnetic order, a finite magnetization magnitude can be established; whereas in environments where the orientations differ significantly over short distances, the magnitudes shrink.

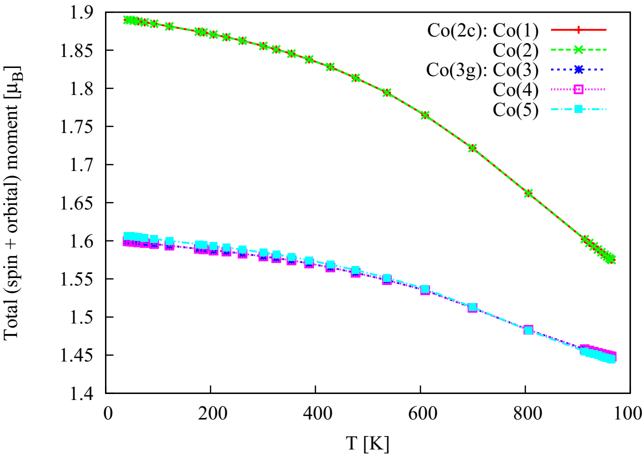

FIG. 4. (Color online) Calculated temperature dependence of the total (including both spin and orbital) local moment for each magnetic sublattice in $YCo_5$.

Figure 4 indicates the extent of this effect in $YCo_5$. We have started with a SDFT calculation of the charge and magnetisation density $\rho(\mathbf{r})$ and $\vec{M}(\mathbf{r})$ for the $T = 0$ K ferromagnetic state $\{\hat{\mathbf{e}} = \hat{\mathbf{n}}\}$ and find the magnetization magnitude per site is 1.9 and $1.6\mu_B$ for the Co($2c$) and Co($3g$) sites, respectively. When we use the self-consistent field potentials that these produce in a frozen potential approximation in our DLM theory for increasing temperatures when the moment orientations become disordered, the average magnetization magnitude per site output from this calculation diminishes. For temperatures up to ∼600 K, this decrease is slight, and thereafter more significant as seen in the figures. Up to 600 K, therefore, the DLM theory as applied is adequate and we can examine the effects of transverse fluctuations on the MAE that it describes. For higher temperatures, however, the effects of short-ranged correlations among the $\hat{\mathbf{e}}$ orientation (via the use of the nonlocal CPA, for example [37,38]) and longitudinal fluctuations [40] need to be addressed for a more complete picture. Comprehensive analyses on bcc-Fe, where the robustness of the local moments are established, can be found in a recent work [41].

Further details about the calculations are described in the Appendix.

## III. RESULTS

We start with the calculated MAE near the ground state to demonstrate its sensitivity to the filling of the electrons in Fig. 2. Corresponding data for the magnetization is shown in Fig. 5. We see that even the sign of the MAE sensitively changes depending on a fraction in the filling of electrons, which is reasonable in the physics of magnetic anisotropy where adding/removing one electron in an electronic cloud that points to a particular real-space direction in a given

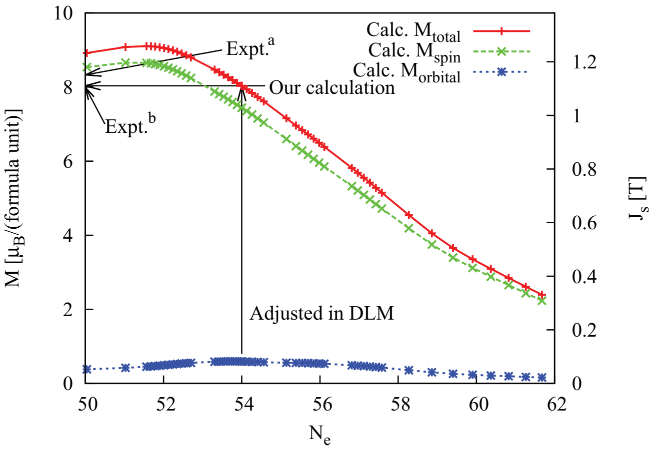

FIG. 5. (Color online) Calculated magnetization of $YCo_5$ plotted as a function of the number of electrons near the ground state at $m = 0.967$. Our calculated result $8.03\mu_B$ at around $T = 100$ K falls onto the experimental numbers within two digits. For the closeness of such data to the ground state, see Fig. 7 (a, $M = 8.33\mu_B$ at liquid-helium temperature from Ref. [23] and b, $M = 7.99\mu_B$ at room temperature from Ref. [26]).

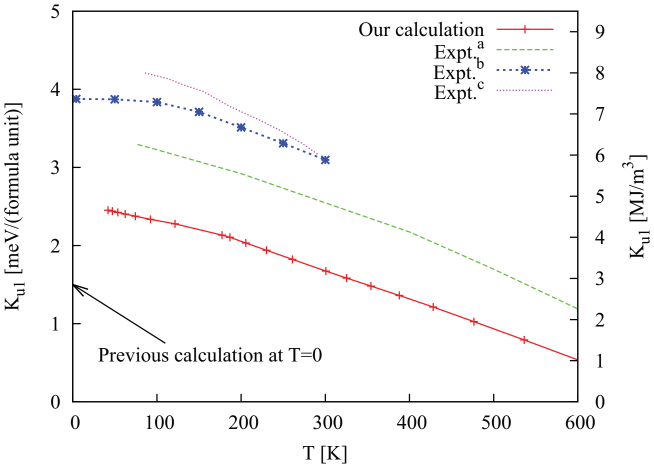

FIG. 6. (Color online) Calculated temperature dependence of magnetic anisotropy energy for $\mathrm{YCo_5}$. Previous calculation result at $T = 0$ is taken from Ref. [27] (a, Ref. [24] for $K_{\mathrm{u1}}$; b, Ref. [23] for $K_{\mathrm{u1}}$; and c, Ref. [25] for $K$, with $K_{\mathrm{u1}}$ dominating).

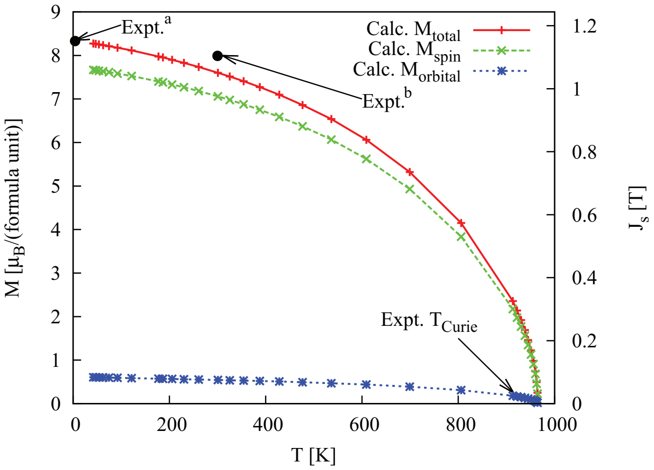

FIG. 7. (Color online) Calculated temperature dependence of magnetization for $\mathrm{YCo_5}$. Experimental Curie temperature, 920 K, is taken from Ref. [26] (a, Ref. [23] and b, Ref. [26]).

crystal-field environment indeed affects which direction the magnetic moment should prefer under the presence of SOI. So the challenge is how precisely we can pinpoint the electron number right onto the realistic one, on which details are given in Sec. A 3 of the Appendix. Fixing the electron number by a fine-tuning of the chemical potential in the DLM runs, we obtain the temperature dependence of MAE and magnetization. The temperature dependence of the anisotropy field is deduced from them. These data for the bulk are shown in Sec. III A. Then we inspect how our calculated MAE scales with respect to the calculated magnetization, resolving into sublattices and temperature ranges in Sec. III B. Comparison to the single ion anisotropy model analyses by Callen and Callen [42] and more recent ones [18,43] is carried out to help uncover the key mechanisms.

### A. Bulk observables

Calculated temperature dependence of MAE for $\mathrm{YCo_5}$ by DLM at the fixed correct valence-electron number is shown in Fig. 6. We have a systematic underestimate of MAE for the overall temperature range as compared to the experimental results found in the literature. However, the qualitative temperature dependence is well reproduced. In a similar manner to MAE, calculated temperature dependence of magnetization at the fixed valence-band filling is shown in Fig. 7. Fitting the calculated temperature dependence of magnetization as it decreases to zero in the temperature range $T > 900$ K to the relation

$$M(T) = A_{\mathrm{M}}|T - T_{\mathrm{Curie}}|^{\beta},$$

we get $T_{\mathrm{Curie}} = 965$ K, $\beta = 0.50$, and $A_{\mathrm{M}} = 0.33$. The critical exponent falls onto the mean-field value $\beta = 1/2$ within the numerical accuracy as it should, which gives a check of the data. Our *ab initio* result for the Curie temperature compares with the experimental Curie temperature $T_{\mathrm{Curie,expt.}} = 920$ K [26] within the deviation of 5%. A mean-field result on the transition temperature typically gives an overestimate by $O(10)\%$ as was observed for the $\mathrm{L1_0}$-FePt alloy calculated by exactly the same method [18] as the one we utilize here; the apparent absence of such an overestimate might rather indicate the fragility of the local moments close to $T_{\mathrm{Curie}}$.

We obtain the *ab initio* result for the temperature dependence of the anisotropy field $H_{\mathrm{A}}$ as shown in Fig. 8(a) following the simple coherent magnetization rotation picture,

$$K_{\mathrm{u1}} = \tfrac{1}{2} M H_{\mathrm{A}}, \qquad (16)$$

with $K_{\mathrm{u1}}$ and $M$ being the calculated uniaxial MAE in Fig. 6 and magnetization in Fig. 7, respectively. The underestimate by 30% of $K_{\mathrm{u1}}$ on the left-hand side of Eq. (16) leads to a similar underestimate of $H_{\mathrm{A}}$.

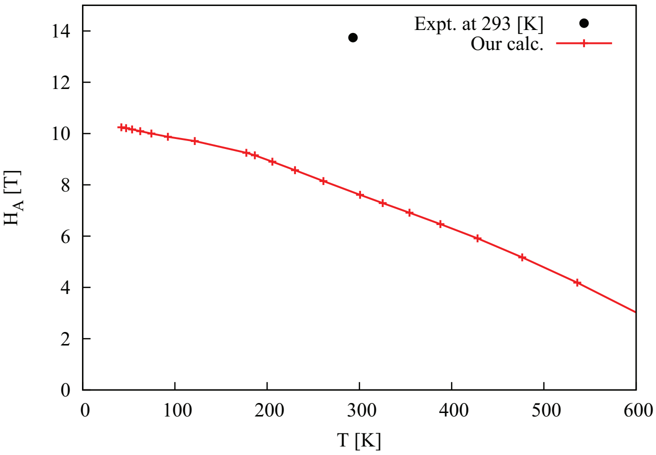

FIG. 8. (Color online) Temperature dependence of the anisotropy field for $\mathrm{YCo_5}$ as deduced from the numbers presented in Figs. 6 and 7, following Eq. (16). The experimental data at 293 K is taken from Ref. [25].

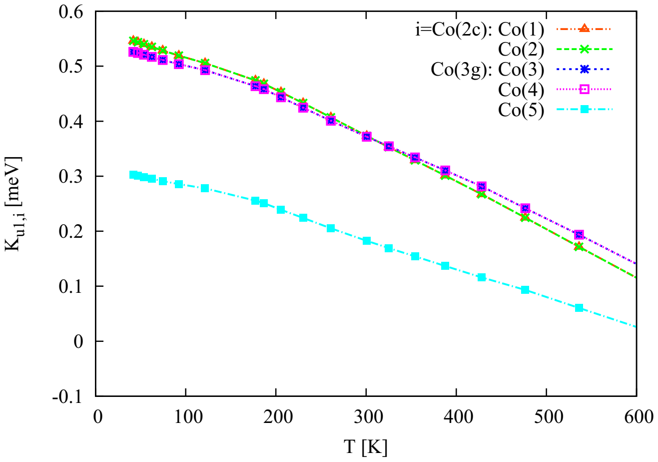

FIG. 9. (Color online) Calculated temperature dependence of local-moment-resolved MAE.

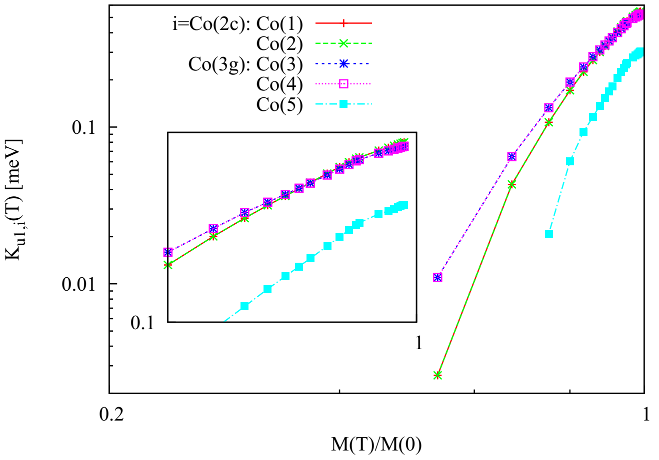

FIG. 10. (Color online) Calculated MAE plotted as a function of the order parameter $m \equiv M(T)/M(0)$ for each local moment $i$. The inset is a zoomed-in plot in region $M(T)/M(0) \lesssim 1$.

### B. Scaling MAE and magnetization

Scaling relation concerning MAE with respect to magnetization

$$K_{u1}(T) = A\,[M(T)/M(0)]^{\alpha} \tag{17}$$

has been discussed for magnetic materials of which the representative one was established by Callen and Callen [42] on the basis of single-ion theory. Their exponent $\alpha = l(l+1)/2$ at low temperatures, where $l$ is the order of the expansion in terms of the spherical harmonics, has been challenged in some materials [18,43]. The Callen-Callen argument for a ferromagnet with the uniaxial anisotropy predicts an exponent $\alpha = 3$ with $l = 2$. Here we inspect what sort of scaling relation holds for our target magnet $YCo_5$. $YCo_5$ is an intermetallic compound and the single-ion theory is not directly applicable to it. On top of that, the particular crystal structure of $YCo_5$ comes with multiple magnetic sublattices in the unit cell. The bulk scaling between MAE and magnetization might not be exactly the same as sublattice-resolved scaling considering the fact that each sublattice is exposed to its own crystal-field environment, depending on its own characteristic temperature dependence.

We start with the temperature dependence of local-moment-resolved MAE as shown in Fig. 9. Exceptional behavior seen for Co(5) in the Co(3$g$) sublattice originates in the effect of SOI with the magnetization direction $\mathbf{n} = (1,0,1)$. Out of the data in Fig. 9, the sublattice-resolved MAE as a function of the order parameter $m = M(T)/M(0)$ is plotted in Fig. 10 to which we apply the scaling relation, Eq. (17), for each of the contributions from the magnetic sublattices as well as for the bulk data. The bulk scaling analysis is shown representatively in Fig. 11. Experimental bulk data is taken from the past literature [23]. For the temperature range where the reliable experimental data set seems to be available, we tabulate the extracted scaling exponents in Table II. The scaling exponents do depend on the magnetic sublattices. We find that the bulk scaling exponent is observed only in a phenomenological way after summing up the contribution of each magnetic atom in the unit cell. The overall calculated trend from the high-temperature side with larger $\alpha$ to the low-temperature side with smaller $\alpha$ is shared by all of the sublattices and the bulk. The bulk scaling exponent around the room temperature is calculated to be $\alpha \sim 5.6$ which reasonably compares with the experimental exponent $\alpha \sim 6.1$ that was extracted in the temperature region including the room temperature.

We note that our calculated data in Fig. 11 shifts from experimental data on the $m$ axis when compared at the same temperatures. Our calculated data for $m > 0.96$ are for below the liquid-nitrogen temperatures while for the experimental data [23] the room-temperature data is already in the parameter range $m > 0.96$. That deviation could be related to the inherent underestimate in our calculations.

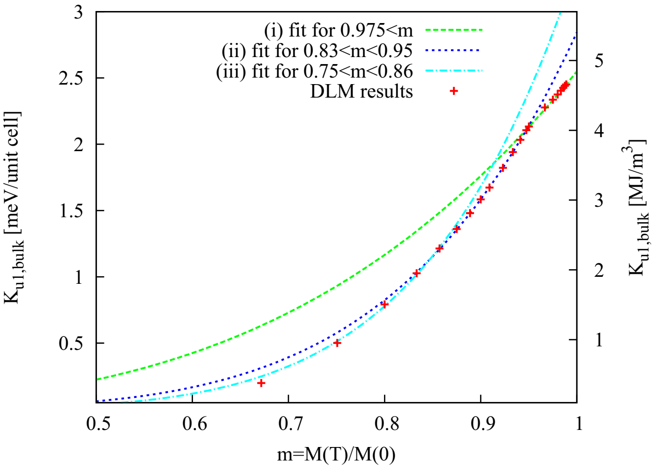

FIG. 11. (Color online) Scaling of the bulk MAE, $K_{u1,\mathrm{bulk}}(T)$, with respect to the order parameter $m = M(T)/M(0)$. The scaling exponent $\alpha$ in $K_{u1,\mathrm{bulk}}(T) = Am^{\alpha}$ depends on the temperature-dependent scaling region: (i) $\alpha = 3.5$ for $m > 0.975$ which corresponds to 41 K $< T <$ 75 K, (ii) $\alpha = 5.6$ for $0.83 < m < 0.95$ which corresponds to 186 K $< T <$ 477 K, and (iii) $\alpha = 6.5$ for $0.75 < m < 0.86$ which corresponds to 428 K $< T <$ 610 K.

TABLE II. Focus temperature range and the extracted scaling exponents $\alpha$ in $K_{u1} \propto m^{\alpha}$ for each local moment on the magnetic sublattice in the unit cell of $YCo_5$ and for the bulk.

| | $T = 177$ K | 186 K | 300 K |
|---|---|---|---|
| Co(1)/Co(2) | – | | $\alpha = 5.6$ |
| Co(3)/Co(4) | – | | $\alpha = 4.9$ |
| Co(5) | | $\alpha = 7.7$ | |
| Bulk (Our calc.) | – | | $\alpha = 5.6$ |
| Bulk (Expt.[a]) | $\alpha = 6.1$ for 150 K $\leqslant T \leqslant$ 300 K | | |

[a] Reference [23].

## IV. DISCUSSIONS

We discuss the strategy to improve the persistence of coercivity against temperature decay. It has been known that the coercivity is approximately proportional to the anisotropy field $H_A$ [5,21]. A significant part of the reduction factor $H_c/H_A$ originates from the microstructure which is beyond the scope of the bulk electronic structure considerations. Now our interest lies in how to improve $H_A(T)$ or equivalently $K_{u1}(T)$ for high $T$. We propose a scheme to exploit the peak position of MAE in Fig. 2 and how the electrons are thermally excited from the ground state following the Fermi-Dirac distribution. The idea is to let the thermally excited electrons populate the targeted electronic state which lies below the peak in Fig. 2 to enhance MCA. For that, we artificially lower the chemical potential to make some place for thermally excited electrons to populate at high temperatures. Then we sacrifice the optimal values of the MCA at low temperatures but we can extract the optimal anisotropy field over the operating temperature ranges.

The results for the calculated temperature dependence of the MAE in the hole-doped $YCo_5$'s is shown in Fig. 12. Hole doping is implemented by artificially lowering the Fermi level in DLM runs for $YCo_5$. Measuring the position of the lowered Fermi level, $E_{F,\text{doped}}$, from the undoped one, $E_{F,\text{undoped}}$, in units of Kelvin helps us to figure out around which temperature range the thermally excited electrons would reach the peak position in Fig. 2. We found that for the reduction range $150\text{ K} \lesssim \Delta_{E_F} \lesssim 300\text{ K}$, with $\Delta_{E_F} \equiv (E_{F,\text{doped}} - E_{F,\text{undoped}})$, some enhancement of the MAE around $T \sim 500$ K is numerically observed. The data with $\Delta_{E_F} = 314$ and 471 K were extracted with the corresponding reduction in the electron number being $\Delta N_e = -0.24$ and $-0.35$, respectively, as the main message of this paper in Fig. 1, where MAE is expressed in terms of the anisotropy field following Eq. (16).

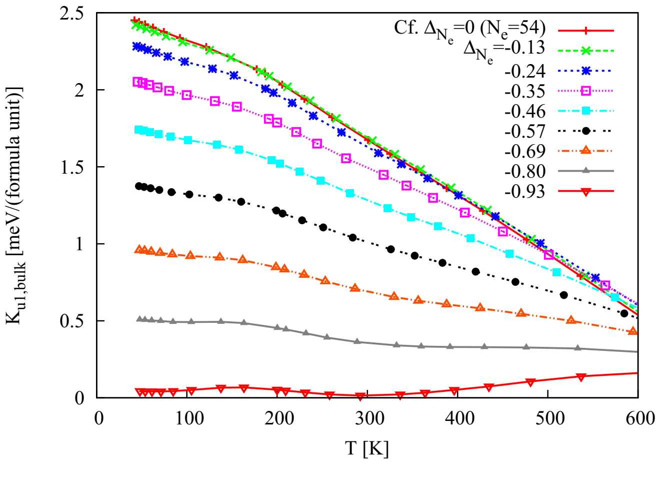

FIG. 12. (Color online) Calculated temperature dependence of MAE for the hole-doped $YCo_5$.

Remarkably, nonmonotonic temperature dependence of $H_A$ is found for the computational "sample" in the low-coercivity region with the electron number reduced by around 0.9 in Fig. 12. This nonmonotonic temperature dependence of MAE is reminiscent of what has been known experimentally for $Y_2Fe_{14}B$ since 1986, where the temperature enhancement in MAE in the order of 0.2–0.3 $MJ/m^3$ is observed around $T \sim 300$ K [44]. The common factor among $Y_2Fe_{14}B$ and $YCo_5$ is that $3d$-electron contribution in the MCA of rare-earth magnets is extracted out. The nonmonotonicity in our finite-temperature data for the chemical-potential-controlled $YCo_5$ comes from the following two factors: (a) thermal population of the particular electronic states that corresponds to the peak of MAE in Fig. 2, and (b) various contributions at finite temperatures from multiple sublattices in the unit cell. We speculate that analogous physics may be at work in $Y_2Fe_{14}B$ which would require more extensive computations than those for the present project.

We note that the Curie temperature shifts as the chemical potential is reduced. The temperature dependence of magnetization shifts rather monotonically with respect to the artificially manipulated chemical potential while $K_{u1}(T)$ behaves nonmonotonically, and the high-temperature enhancement seen in Figs. 1 and 12 is to be considered as a finite-temperature reflection of the nonmonotonic ground-state behavior in Fig. 2 rather than a reflection of the plain shift of the Curie temperature.

## V. CONCLUSIONS

The temperature dependence of MAE and the magnetization for $YCo_5$ has been calculated from first principles within the assumption of local moments to give the qualitative agreement with the experimental data. We have proposed a way to improve the high-temperature coercivity by hole doping as was demonstrated by calculations with the filling controlled by the chemical potential manipulation. That can be implemented as applying the gate voltage for the case of a thin film sample, or alloying Co with some other elements to slightly reduce the valence electron number in the bulk. Since Co is an expensive element, replacing it with some cheaper ingredients with the improved coercivity in the practical operation temperature range is quite welcome. Thus we have proposed a way to improve the practical utility of $YCo_5$ from the perspective of the electronic structure and statistical physics.

## ACKNOWLEDGMENTS

This work is supported by the Elements Strategy Initiative Center for Magnetic Materials (ESICMM) under the outsourcing project of the Ministry of Education, Culture, Sports, Science and Technology (MEXT), Japan. Support is acknowledged from the EPSRC (UK) Grant No. EP/J006750/1

(J.B.S. and R.B.). Overall guidance given by T. Miyake and H. Akai is gratefully acknowledged. M.M. thanks ESICMM researchers and Y. Yamaji for helpful discussions, L. Petit and D. Paudyal for fruitful interactions during the KKR workshop in Warwick in July 2013, O. N. Mryasov for discussions during his visit to ESICMM, NIMS in July-August 2013, and K. Hono for the overall push to the present project. Numerical computations were performed on "Minerva" at University of Warwick and SGI Altix at National Institute for Materials Science.

## APPENDIX: DETAILS OF THE CALCULATIONS FOR YCo$_5$

### 1. Adjustment of the valence electron number

The overall calculation consists of two steps:

(1) The first step is to generate the grand potentials for each of the assumed local-moment configurations by a scalar-relativistic KKR calculation. We do a spin-polarized calculation for YCo$_5$ as parametrized by Vosko *et al.* [45] to reach the ferromagnetic ground state and yield the potentials for each local moment on the magnetic sublattices.

(2) Then the second step consists of solving the fully relativistic equation of state under the potentials generated by the electronic structure calculation in step 1 and the direction of magnetization is fixed to be $\mathbf{n} = (1,0,1)$ with the motivation to address MAE using the torque-based formula in Eq. (15). Solutions are obtained so that Eqs. (3) and (5) are solved self-consistently to yield the results on MAE, magnetization, and the temperature. In these KKR-based calculations we set the cutoff order in the expansion of spherical harmonics $l_{\max} = 3$ all through the above two steps.

In step 1, we follow the atomic-sphere approximation (ASA) considering the deformed shape of the unit cell to avoid the complication caused by overlapping muffin-tin spheres or too large an interstitial region. We have confirmed that this ASA construction is adequate from full-potential (FP) linear muffin-tin orbital (LMTO) calculations where we find the ASA and FP-LMTO densities of states for the $T = 0$ K cases to compare well.

Having a difference in the treatment of the SOI between steps 1 and 2, an adjustment of the Fermi level needs to be done to exactly fix the number of electrons, which is demonstrated in Fig. 13. The adjustment is done in the order of $O(0.01)$ (Ry) $\sim O(0.001)$ (eV). We describe the practical procedure for this in Sec. A 3 of the Appendix.

### 2. Achieving the self-consistency in DLM with multiple magnetic sublattices in the unit cell

Further iterations within DLM is taken for YCo$_5$ to achieve the self-consistency of the calculation to incorporate the effects of multiple mean fields that depend on the magnetic sublattice within the unit cell. The target material YCo$_5$ has at least two different magnetic sublattices, Co($2c$) and Co($3g$), and the magnetic moments on them can be different from each other as was found in the neutron scattering experiments [26]. The Weiss fields are obtained from Eqs. (3) and (5) solved self-consistently for the sites on the sublattice where there are local moments residing. We proceed as follows.

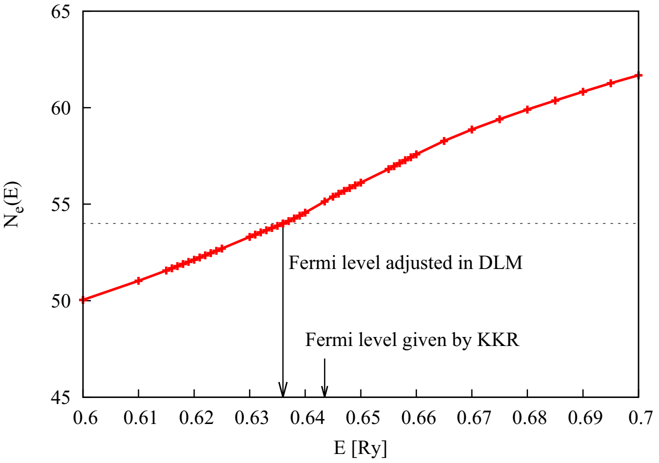

FIG. 13. (Color online) Calculated Fermi-level dependence of the number of electrons for pure YCo$_5$ near the ground state at $m = 0.967$ [$m = L(\beta h)$ with $\beta h = 30$ as in Eq. (8)]. Equation of state is solved with the artificially given Fermi level to adjust the valence electron number exactly to the number as set up by the calculation.

(1) We start with a run with $\beta h$ uniformly set over all of the local moments in the unit cell so that $m_i = L(\beta h)$. We refer to this run as the zeroth round of the correction process.

(2) With the output of the zeroth round, the input $\beta h$'s are reset by using the output Weiss fields produced by the calculation from Eq. (3):

$$\beta = (\beta h)_i / h_i \tag{A1}$$

for all $i$'s. We note that the left-hand side, inverse temperature, is sublattice independent. This imposes the self-consistency condition: We fix the input $\beta h$ for the Co($2c$) sublattice and adjust $\beta h$ for other local moments that sit on the other sublattices according to the following relation:

$$\frac{(\beta h)_{\mathrm{Co}(3g)}}{h_{\mathrm{Co}(3g)}} \equiv \frac{(\beta h)_{\mathrm{Co}(2c)}}{h_{\mathrm{Co}(2c)}}. \tag{A2}$$

Using the output of the zeroth round for $h$'s, the input numbers for $(\beta h)_{\mathrm{Co}(3g)} = h_{\mathrm{Co}(3g)}(\beta h)_{\mathrm{Co}(2c)}/h_{\mathrm{Co}(2c)}$ is used for the first round.

(3) The process is iterated, making the second, third, ... rounds in the correction process, until the input $S^1$ and the output $S^1$'s are identical within the numerical accuracy.

We have observed that for $(\beta h)_{\mathrm{Co}(2c)} \geqslant 10$ the convergence within four digits for $h$'s is quickly reached typically after three iterations while for $(\beta h)_{\mathrm{Co}(2c)} \gtrsim 0.1$ the convergence takes around ten iterations. The iteration can run into a limit cycle of a few periods beyond the fifth digit of $\beta h$. At such stage of the iteration, we note that the convergence was reached within the numerical precision of four digits for $S^1$ which we believe is sufficient.

### 3. Determining and varying the chemical potential in the DLM

In addressing magnetic hardness from first principles, MAE needs to be calculated as precisely as possible. The behavior of the calculated MAE as a function of the valence electron number for YCo$_5$ is shown in Fig. 2. This data is obtained in a series of DLM runs by artificially modulating the chemical potential near the ground state. Here the data near the ground state means the order parameter is fixed to be $m = 0.967 = L(\beta h)$ with $\beta h = 30$. MAE has a strong dependence on the electron filling and only after fixing the electron number by a fine-tuning of the chemical potential in the DLM run, can we discuss the temperature dependence of MAE and magnetization from first principles: Here we fix the valence electron number down to four digits by manually tuning the chemical potential. The fine-tuning follows Newton's method in spirit, where we keep on shifting the chemical potential by $\Delta\mu$ with

$$\Delta\mu = (N_{e,\text{desired}} - N_e)/n(\mu),$$

where $N_e$ is the electron number given as $N^{(\hat{\mathbf{n}})}(\mu)$ and $n(\mu)$ is the density of states at $\mu$, until the desired electron number $N_{\text{desired}} = 54$ is numerically reached by iterating the calculations with the shifted chemical potential $(\mu + \Delta\mu)$. At this determined chemical potential and the electron number $N_e = 54.00$ near the ground state, we find the low-temperature MAE to be 2.3 meV/unit cell as shown in Fig. 2. Using the experimental lattice constants [26], this is equivalent to 4.4 MJ/m$^3$, which compares with the experimental result at liquid-nitrogen temperature, 6.3 MJ/m$^3$ [24], with an underestimate of 30%.

The above fine-tuning of the chemical potential also depends on the temperature. At each data point on the temperature axis, the valence electron number is fixed to be 54.00 within the numerical accuracy which practically gives a temperature-dependent chemical potential from 0.636 09 Ry at the lowest temperatures to 0.633 57 Ry at the calculated highest temperature 965 K.

### 4. Magnetization and local moments

The total magnetization, and its spin part and the orbital part, is calculated to be 8.03$\mu_B$, 7.44$\mu_B$, and 0.59$\mu_B$, respectively, as shown in Fig. 5 for low temperature. The calculated total magnetization amounts to $J_s = 1.11$ T using the experimental lattice constants [26]. These results agree with the experimental numbers found in the literature of 7.99$\mu_B$ [26] or $J_s = 1.1$ T [8] within 0.5%.

TABLE III. Calculated magnitude of local moments in $\mu_B$. Experimental numbers are taken from Ref. [26].

| | Total | Spin | Orbital |
|---|---|---|---|
| Co(2$c$) (our calc.) | 1.88 | 1.81 | 0.0667 |
| Co(2$c$) (expt.) | 1.77 | 1.31 | 0.46 |
| Co(3$g$) [our calc. for Co(3)/Co(4)] | 1.59 | 1.44 | 0.150 |
| [our calc. for Co(5)] | 1.60 | 1.44 | 0.164 |
| Co(3$g$) (expt.) | 1.72 | 1.44 | 0.28 |

However, we note that this apparent excellent agreement is actually realized by a cancellation of overestimates and underestimates, which is revealed by inspecting each local moment's contribution to the total magnetization. At the fixed filling, our results are extracted as summarized in Table III. Our calculated local moments on the Co(2$c$)/Co(3$g$) sublattices are 1.88 and 1.59$\mu_B$ which compare with the results from neutron experiments 1.77/1.72$\mu_B$ [26] within 6%–8%. Those polarizations are given by DLM in the fully relativistic calculation near the ground state, based on the potentials generated by the scalar-relativistic KKR calculation at $T = 0$ which gave the polarization as 1.48 and 1.52 for Co(2$c$) and Co(3$g$), respectively. In the present local-moment approach for YCo$_5$ we have systematic underestimate of the orbital moments compared with the neutron measurements. However, the resolution of the neutron data into spin and orbital contributions also involves some subtlety [46]. The accurate *ab initio* estimation of the orbital contribution to the magnetization is left for future projects.

---

[1] W. F. Brown, Rev. Mod. Phys. **17**, 15 (1945).
[2] M. Sagawa, S. Fujimura, N. Togawa, H. Yamamoto, and Y. Matsuura, J. Appl. Phys. **55**, 2083 (1984).
[3] Y. Tawara and H. Senno, Jpn. J. Appl. Phys. **7**, 966 (1968).
[4] E. A. Nesbitt, R. H. Willens, R. C. Sherwood, E. Buehler, and J. H. Wernick, Appl. Phys. Lett. **12**, 361 (1968).
[5] H. Kronmüller, K. D. Durst, and M. Sagawa, J. Magn. Magn. Mater. **74**, 291 (1988).
[6] K. Hono and H. Sepehri-Amin, Scr. Mater. **67**, 530 (2012).
[7] R. Skomski, J. Appl. Phys. **83**, 6724 (1998).
[8] K. Ohashi, J. Jpn. Inst. Met. **76**, 96 (2012).
[9] K. Strnat, G. Hoffer, J. Olson, W. Ostertag, and J. J. Becker, J. Appl. Phys. **38**, 1001 (1967).
[10] J. Hubbard, Phys. Rev. B **19**, 2626 (1979).
[11] H. Hasegawa, J. Phys. Soc. Jpn. **46**, 1504 (1979).
[12] J. Hubbard, Phys. Rev. B **20**, 4584 (1979).
[13] J. Hubbard, Phys. Rev. B **23**, 5974 (1981).
[14] A. J. Pindor, J. Staunton, G. M. Stocks, and H. Winter, J. Phys. F: Met. Phys. **13**, 979 (1983).
[15] B. L. Gyorffy, A. J. Pindor, J. Staunton, G. M. Stocks, and H. Winter, J. Phys. F: Met. Phys. **15**, 1337 (1985).
[16] J. Staunton, B. L. Gyorffy, A. J. Pindor, G. M. Stocks, and H. Winter, J. Phys. F: Met. Phys. **15**, 1387 (1985).
[17] J. Staunton, B. L. Gyorffy, G. M. Stocks, and J. Wadsworth, J. Phys. F: Met. Phys. **16**, 1761 (1986).
[18] J. B. Staunton, S. Ostanin, S. S. A. Razee, B. L. Gyorffy, L. Szunyogh, B. Ginatempo, and E. Bruno, Phys. Rev. Lett. **93**, 257204 (2004).
[19] J. B. Staunton, L. Szunyogh, A. Buruzs, B. L. Gyorffy, S. Ostanin, and L. Udvardi, Phys. Rev. B **74**, 144411 (2006).
[20] A. Buruzs, P. Weinberger, L. Szunyogh, L. Udvardi, P. I. Chleboun, A. M. Fischer, and J. B. Staunton, Phys. Rev. B **76**, 064417 (2007).
[21] S. Hirosawa, K. Tokuhara, Y. Matsuura, H. Yamamoto, S. Fujimura, and M. Sagawa, J. Magn. Magn. Mater. **61**, 363 (1986).
[22] K. Hono and S. Hirosawa, Magnetics Japan **7**, 290 (2012).

[23] J. M. Alameda, D. Givord, R. Lemaire, and Q. Lu, J. Appl. Phys. **52**, 2079 (1981).

[24] K. H. J. Buschow, A. M. van Diepen, and H. W. de Wijn, Solid State Commun. **15**, 903 (1974).

[25] L. Pareti, O. Moze, M. Solzi, and F. Bolzoni, J. Appl. Phys. **63**, 172 (1988).

[26] J. Schweizer and F. Tasset, J. Phys. F: Met. Phys. **10**, 2799 (1980).

[27] P. Larson and I. I. Mazin, J. Appl. Phys. **93**, 6888 (2003).

[28] K. H. J. Buschow and M. Brouha, J. Appl. Phys. **47**, 1653 (1976).

[29] J. Korringa, Physica **13**, 392 (1947).

[30] W. Kohn and N. Rostoker, Phys. Rev. **94**, 1111 (1954).

[31] P. Soven, Phys. Rev. **156**, 809 (1967).

[32] H. Ebert, D. Ködderitzsch, and J. Minár, Rep. Prog. Phys. **74**, 096501 (2011).

[33] G. M. Stocks, W. M. Temmerman, and B. L. Gyorffy, Phys. Rev. Lett. **41**, 339 (1978).

[34] J. S. Faulkner and G. M. Stocks, Phys. Rev. B **21**, 3222 (1980).

[35] P. Lloyd and P. R. Best, J. Phys. C **8**, 3752 (1975).

[36] P. Strange, J. Staunton, and B. L. Gyorffy, J. Phys. C **17**, 3355 (1984).

[37] A. Marmodoro, A. Ernst, S. Ostanin, and J. B. Staunton, Phys. Rev. B **87**, 125115 (2013).

[38] J. B. Staunton, A. Marmodoro, and A. Ernst, J.Phys.: Condens. Matter **26**, 274210 (2014).

[39] J. B. Staunton and B. L. Gyorffy, Phys. Rev. Lett. **69**, 371 (1992).

[40] M. Uhl and J. Kübler, Phys. Rev. Lett. **77**, 334 (1996).

[41] A. Deák, E. Simon, L. Balogh, L. Szunyogh, M. dos Santos Dias, and J. B. Staunton, Phys. Rev. B **89**, 224401 (2014).

[42] H. B. Callen and E. Callen, J. Phys. Chem. Solids **27**, 1271 (1966).

[43] O. N. Mryasov, U. Nowak, K. Y. Guslienko, and R. W. Chantrell, Europhys. Lett. **69**, 805 (2005).

[44] S. Hirosawa, Y. Matsuura, H. Yamamoto, S. Fujimura, and M. Sagawa, J. Appl. Phys. **59**, 873 (1986).

[45] S. H. Vosko, L. Wilk, and M. Nusair, Can. J. Phys. **58**, 1200 (1980).

[46] K. Saito (private communication).